A SELECTION OF RECENT CLEO RESULTS: B PHYSICS, SILICON DETECTOR, AND MORE...

Roy A. Briere*
Harvard University
HEP Lab, 42 Oxford St.
Cambridge, MA 02138

Representing the CLEO Collaboration

ABSTRACT

Some recent results from the CLEO experiment are reviewed. The first portion highlights our efforts studying the CKM matrix with measurements of semi-leptonic B decays and our comprehensive survey of rare B decay modes. Next, some of the first results from our new silicon vertex detector are presented, along with a glimpse of related ongoing analyses. Finally, a few examples of the excellent physics CLEO does outside the B system are mentioned.

*Supported by DOE Grant DE-FG02-91ER40654.

1 Introduction

The CLEO detector operates at the Cornell Electron Storage Ring. This 768 meter ring is filled with electrons and positrons, each comprising nine trains of three bunches with a current of more than 200 mA/beam. The trains are 300 ns apart, while bunches are 28 ns apart within each train. Out peak luminosity now exceeds $6 \times 10^{32}\mathrm{cm}^{-2}\mathrm{s}^{-1}$; this surpasses our most recent goal and is the highest at any collider. The most luminosity actually logged to tape by CLEO in one day (month) is 30 (480) pb^{-1}.

After detector and accelerator upgrades are completed in 1999, CESR will run with nine trains of five bunches at a 14 ns bunch spacing. The goal is peak luminosities of $1.7 \times 10^{33}\mathrm{cm}^{-2}\mathrm{s}^{-1}$, yielding 15 fb^{-1} per year with a realistic operating schedule.

CESR has run on all of the Υ resonances in the past. The $\Upsilon(4S)$ is special, being just above $B\bar{B}$ threshold. Standard running now includes only two energies: on the $\Upsilon(4S)$ resonance and in the continuum region just below it.

The off-resonance, or "continuum" energies are typically 60 MeV below the $\Upsilon(4S)$ peak, at $E_{cm} = 10.52$ GeV. The hadronic cross-section is about 3 nb. Fermion-anti-fermion pairs are produced in the decay of one 10.6 GeV off-shell photon at rest: $e^+e^- \to \gamma^\star \to \tau^+\tau^-, c\bar{c}$, etc. Processes such as two-photon collisions, $\gamma\gamma \to X$, also occur.

The on-resonance, or "On4S," running takes place at $E_{cm} = 10.58$ GeV. The effective cross-section for $\Upsilon(4S)$ production is almost 1.1 nb. The reaction $e^+e^- \to \Upsilon(4S) \to B\bar{B}$ results in the decay of two 5.28 GeV B mesons almost at rest. This process is also accompanied by all the continuum processes listed above. The $B\bar{B}$ portion is partly separable via event shape. The jetty hadronization of quark jets is usually quite distinct from the round symmetric decay of two slow B mesons. One can also use the off-resonance data to study backgrounds to the $B\bar{B}$ sample.

Two-thirds of our luminosity is taken On4S. With this ratio, 1.4 fb^{-1} total (On4S + continuum) data yields 10^6 $B\bar{B}$ pairs or equivalently 10^6 B^+ and 10^6 $\bar{B}^0$. The *total* luminosity of the data used for each of our results will be quoted.

Please note that all results not yet published are preliminary and hence subject to minor changes.

2 The CLEOII Detector

The CLEOII.V detector is shown in Fig. 1. The basic detector characteristics are summarized below; more information may be found in the references.[1,2]

CLEO has tracking over more than 90% of 4π in a solenoidal field, B = 1.5 Tesla. Tracks curl inside the chamber for $p_T < 250$ MeV/c; the resolution is $\sigma_p/p \sim 0.6\%$ at 2 GeV/c. Specific ionization information (dE/dx) from 49 of the wire chamber layers gives K/π separation of about 2σ for 2.6 GeV/c (the momentum of stiff tracks from interesting rare two-body B decays).

Particle identification (PID) is supplemented by a Time-of-Flight (TOF) system. The resolution of the barrel system is about 150 ps; TOF separation of πs and Ks deteriorates for momenta greater than about 1 GeV/c.

Our calorimeter consists of 7800 CsI(Tl) crystals located in a barrel inside the super-conducting magnet coil and in two endcaps and covers 98% of 4π. The best barrel section, with the least material in front of it, comprises 70% of the coverage. Here, the typical π^0 mass resolution is 6 MeV.

The Muon ID system consists of iron absorbers interspersed with streamer counters covering 85% of the solid angle. The efficiency turn-on for a five interaction length penetration cut is at 1.4 GeV/c, with 1% fakes.

The pre-SVX CLEOII detector, featuring the new CsI calorimeter, operated from 1989-1995, collecting 5 fb^{-1} of data. Many discoveries were made with this data. During this era, CESR saw many innovations in its running, including the transition to one interaction region, pretzel orbits, a crossing angle, and multi-bunch operations. All of this data is now re-analyzed; tracking in particular is improved.

The start of the CLEOII.V era in 1995 is marked by the installation of our first silicon vertex detector (SVX), also the first to be operated at the $\Upsilon(4S)$. The upgrade included a new beam pipe and interaction region. The main drift chamber gas was changed from 50-50% Ar-C_2H_6 to 60–40% He-C_3H_8; this reduces multiple scattering and the Lorentz angle which improved resolution and efficiency.[3] Running over the period 1995-1999 will produce over 8 fb^{-1} of physics data; more than 7 fb^{-1} is already on tape as of October 1998.

The CLEOIII upgrade, scheduled for installation in 1999, includes a Ring-Imaging Cherenkov (RICH) detector for greatly improved particle identification. In addition, a new drift chamber, silicon vertex detector, beam pipe and interaction region will be installed. The concurrent CESR machine upgrade includes super-conducting RF cavities,

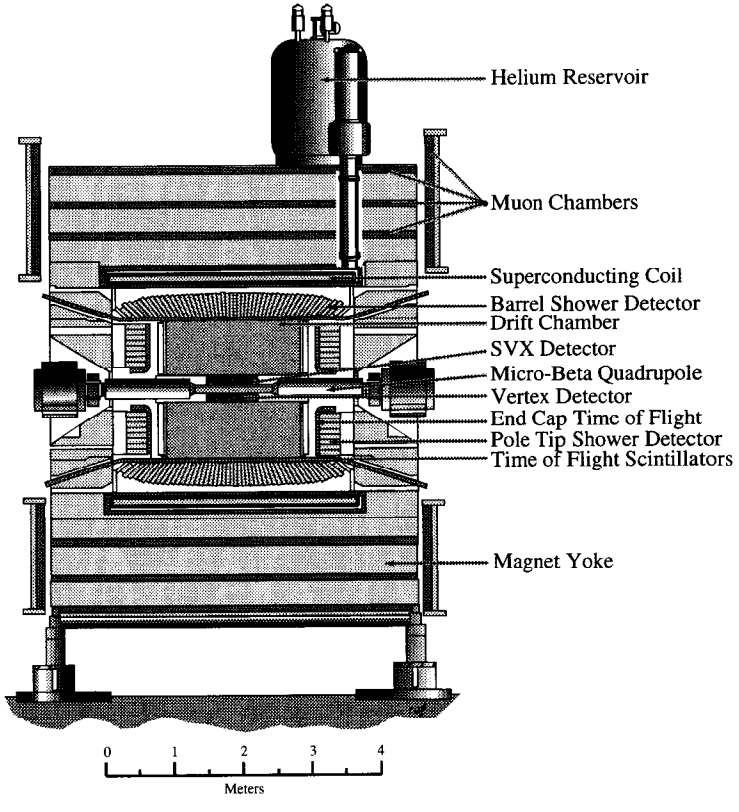

Fig. 1. The CLEOII.V Detector.

and new super-conducting focusing quadrupoles. CLEO expects to collect 15 fb^{-1} of data per year.

3 Kinematics at the $\Upsilon(4S)$

CESR has symmetric beam energies such that the energy of B mesons is given by $E_B = E_{beam}$, where E_{beam} is well-known from accelerator parameters. The average B meson momentum is quite small, $|P_B| \simeq 325$ MeV/c.

When all daughters of the decay are measured, there are two very useful variables. The first is (sums are over daughter particles):

$$\Delta E \equiv \sum E_i - E_{beam}. \tag{1}$$

This simply expresses energy conservation, peaking at zero for real events. It is sensitive to missing particles and also to K-π mis-identification which both affect the energy. A typical resolution is about 25 MeV for $D\pi$; however, it is much improved, to 8 MeV, for final states like $D^{*+}D^{*-}$ and $D\bar{D}\bar{K}$ with large rest-mass. The second key variable is the "beam-constrained" mass:

$$M_B \equiv \sqrt{E_{beam}^2 - |\sum \vec{P}_i|^2}. \tag{2}$$

This expresses momentum conservation. Using E_{beam} instead of $\sum E_i$ improves the mass resolution by a factor of 10, to 2.5 MeV, for two-body modes like $D\pi$.

Often these are the final two variables examined for a peaked excess indicative of a signal. This technique is used extensively for hadronic decays where the decay products are generally all accessible as charged tracks and photons. It is also used for some semi-leptonic modes; this is possible when the neutrino is inferred from global four-momentum balance. More details will be given below when discussing $|V_{ub}|$.

Another variant on the full reconstruction may be termed semi-inclusive reconstruction. Part of the final state is common to all channels, but a varying number of other particles are added in order to find the best B candidate. This is used, for example, in the $b \to s\gamma$ analysis discussed later, where one requires a stiff photon, a kaon, and a varying number of added pions.

There are many other techniques commonly used at CLEO, for example, partial reconstruction of a D^{*+} from the slow transition π^+ only, but there is not time to discuss these further.

4 Magnitudes of CKM Matrix Elements at CLEO

Recall the basic pattern of CKM mixing:

$$\begin{pmatrix} |V_{ud}| & |V_{us}| & |V_{ub}| \\ |V_{cd}| & |V_{cs}| & |V_{cb}| \\ |V_{td}| & |V_{ts}| & |V_{tb}| \end{pmatrix} \sim \begin{pmatrix} 1 & \lambda & \lambda^3 \\ \lambda & 1 & \lambda^2 \\ \lambda^3 & \lambda^2 & 1 \end{pmatrix} \quad (3)$$

where only the approximate magnitudes by order in the parameter $\lambda = \sin\theta_C \simeq 0.22$ are shown.

CLEO does best at measuring $|V_{ub}|$ from $B \to \pi\ell\nu$, with theory to normalize the form factor, and $|V_{cb}|$ from $B \to D^*\ell\nu$ with HQET to constrain the form factor. CLEO can also, in principle, very cleanly get $|V_{ub}|$ from $B \to \ell\nu$, but the very small rate will make the mere observation of this process difficult.

CLEO has also measured $B\bar{B}$ mixing, which scales with $|V_{td}|^2$, while the $b \to s\gamma$ process can yield some information on $|V_{ts}|$. The ratio $|V_{td}/V_{ts}|$ will eventually be accessible from the comparison of $B \to \rho\gamma$ and $B \to K^*\gamma$, but the former process remains undetected and only a limit on $|V_{td}/V_{ts}|$ is possible. Competing limits are available elsewhere from comparisons of B_s and B_d mixing.

We will return to the issue of phases of the CKM matrix elements, such as V_{ub} and V_{td}, later. First, some recent results involving the magnitudes are surveyed.

4.1 Introduction to Semi-Leptonic B Decays

Given the $V-A$ structure of the weak interaction and the fact that leptons do not interact strongly with the hadronic decay products, semi-leptonic decays, such as $B \to D^{(*)}\ell\nu$, are almost as simple as two-body decays. The only complication is that q^2, the $\ell - \nu$ invariant mass, is not fixed. The non-trivial dependences of the matrix element on q^2 are contained in functions known as form factors.

One often replaces q^2 with the HQET-inspired variable

$$w = (M_B^2 + m_M^2 - q^2)/2M_B m_M \quad (4)$$

for $B \to M\ell\nu$ decay, which is just the Lorentz γ of the meson M in the B rest-frame. Clearly, $w = 1$ corresponds to q^2_{max} where M is at rest ('zero-recoil'), and the ℓ and ν are back to back while w_{max} corresponds to $q^2 = 0$ where M recoils against the $\ell\nu$ system.

The form-factors are often parameterized as:

$$\mathcal{F}(w) = \mathcal{F}(1) \times (1 - \hat{\rho}^2(w-1) + c(w-1)^2 + ...). \quad (5)$$

There is one relevant form factor for $P\ell\nu$ and three for $V\ell\nu$, where P and V represent pseudo-scalar and vector mesons, respectively, such as the D and D^*. One can use HQET to inter-relate the form factors if desired.

One important feature of semi-leptonic decays is Luke's Theorem: there are no $1/m_b$ corrections in HQET at q^2_{max} for the $D^*\ell\nu$ process. Note that this is *not* true for other q^2 or for $D\ell\nu$. Of course, nature is not overly kind, and experiments suffer from lower rates and efficiencies and higher backgrounds at q^2_{max}.

Lattice QCD calculations promise to offer increasing precision on the form factor for $B \to D\ell\nu$, these studies faring better for the ground-state D rather than D^*. Once again Nature confounds us somewhat since experiments suffer higher background, notably from D^* and D^{**} feed-down, a lower branching ratio, and proportionately less rate near zero recoil for $D\ell\nu$ relative to $D^*\ell\nu$.

Measurements of V_{ub} are even more difficult for experimenters due to low rates and high backgrounds, and also for theorists. On the lattice, the low energy scale is troublesome, while off the lattice, the niceties of HQET are now absent. Nonetheless, reliable results have been extracted; these more recent achievements are presented first.

4.2 Measurements of $|V_{ub}|$

The $b \to u$ transition was first observed at CLEO by studying the lepton momentum spectrum near the kinematic endpoint. Leptons from these transitions can have momenta beyond the $b \to c$ endpoint. Since only a tiny fraction of the spectrum is examined, model-dependence is the dominant error in the most recent such result:[4]

$$|V_{ub}/V_{cb}| \simeq 0.06 - 0.10. \quad (6)$$

A newer neutrino-reconstruction technique enabled CLEO to observe the exclusive semi-leptonic $b \to u$ final states $\pi\ell\nu$, $\rho\ell\nu$, and $\omega\ell\nu$. The neutrino four-momentum is inferred from the known beam energy and careful measurement of all tracks and unmatched showers in the rest of the event (both Bs). Exactly one lepton is required, so that only one neutrino is missing, and good charge-balance among the tracks is enforced. Care is taken to avoid mistaking hadronic shower fragments for photons to prevent double-counting. After much hard work, the resolution on the inferred neutrino

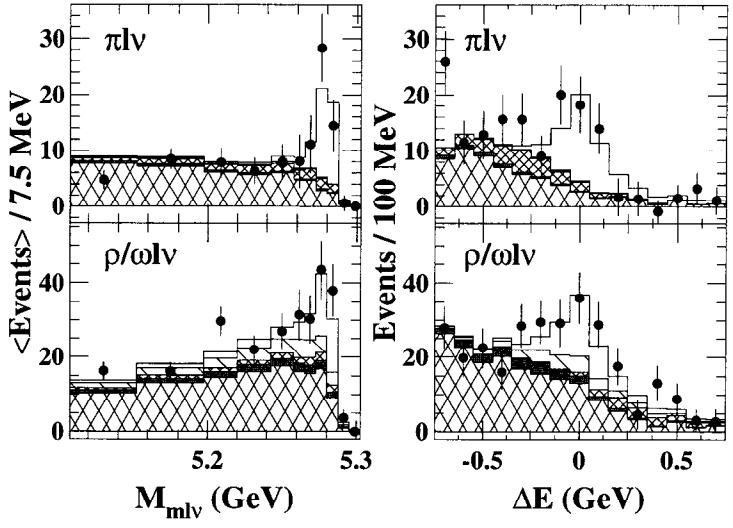

Fig. 2. The beam-constrained mass and energy-balance distributions for the $\pi\ell\nu$ and $\rho/\omega\ell\nu$ modes. The points with errors represent the data after continuum and fake subtraction, and the histogram is the total fit to the data. The open area under the histogram represents the signal component, and the various shaded areas are backgrounds, including cross-feed among modes and feed-down from other $b \to u\ell\nu$ processes. The largest background, from $b \to cX$, is cross-hatched.

is excellent, $\sigma_{p_\nu} \sim 110$ MeV/c. With the neutrino in hand, full reconstruction of the B meson is possible. The resulting ΔE and M_B distributions are displayed in Fig. 2.

The results from 4 fb^{-1} of CLEOII data are:[5]

$$\mathcal{B}(B \to \pi^-\ell^+\nu) = (1.8 \pm 0.4(stat) \pm 0.3(syst) \pm 0.2(model)) \times 10^{-4}, \quad (7)$$

$$\mathcal{B}(B \to \rho^-\ell^+\nu) = (2.5 \pm 0.4(stat)^{+0.5}_{-0.7}(syst) \pm 0.5(model)) \times 10^{-4}, \quad (8)$$

$$|V_{ub}| = (3.3 \pm 0.2^{+0.3}_{-0.4} \pm 0.7) \times 10^{\ 3}, \quad (9)$$

where isospin constraints are employed between the two $\pi\ell\nu$ modes and the three $\rho\ell\nu, \omega\ell\nu$ modes, leading to the extraction of two average branching ratios.

The limiting factors when extracting $|V_{ub}|$ are a 12% error from the branching ratios, mostly from neutrino reconstruction efficiency, and a 20% model dependence. More statistics will help further constrain the models.

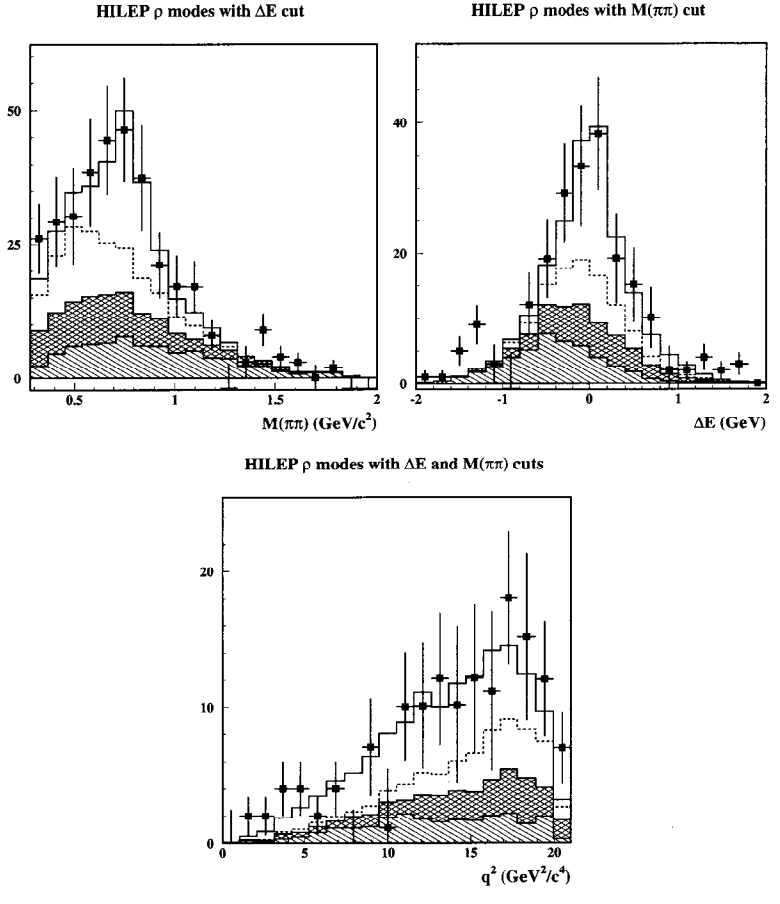

Fig. 3. Preliminary results from the fit to continuum-subtracted data $B \to \rho\ell\nu, \omega\ell\nu$ data in the 2.3–2.7 GeV/c lepton momentum bin. Points are data; the fit is a sum of $b \to c$ (single-hatch), other $b \to u$ (double-hatch), cross-feed (dashed histogram), and signal (solid histogram).

A new $b \to u\ell\nu$ analysis on the full 5 fb^{-1} of CLEOII data is now available. The decays $B \to \rho\ell\nu, \omega\ell\nu$ were measured in an analysis using a simpler, "loose-cut" neutrino reconstruction. Leptons are required to have $p > 1.7$ GeV/c to control background, and the decay kinematics are required to be consistent with the neutrino hypothesis. The most sensitive portion of the momentum spectrum is the so-called "HILEP" bin: leptons from 2.3–2.7 GeV/c. Background comes from other $b \to u$, $b \to c$, and continuum.

The analysis uses a likelihood fit to the 2π or 3π mass (for the ρ or ω channel), ΔE, background levels of other $b \to u$, $b \to c$, continuum, fake ℓ, and finally branching ratios for $\pi^+/\pi^0/\rho^+/\rho^0/\omega\ell\nu$. The $\pi\pi$ mass, ΔE and q^2 distributions are shown in Fig. 3. The preliminary results are:[6]

$$\begin{aligned} \mathcal{B}(B^0 \to \rho^-\ell^+\nu) &= (2.8 \pm 0.4 \pm 0.4 \pm 0.6) \times 10^{-4}, \\ |V_{ub}| &= (3.2 \pm 0.3^{+0.2}_{-0.3} \pm 0.6) \times 10^{-3}, \\ \rho^2 &= 0.52 \pm 0.11 \pm 0.09 \pm 0.05. \end{aligned}$$

These are consistent with the previous neutrino reconstruction results; they also benefit from improved models of $b \to u\ell\nu$ decays spurred by that earlier result.

4.3 Measurements of $|V_{cb}|$

One major goal of studying $b \to c\ell\nu$ processes is the measurement of $|V_{cb}|$. It is also desirous to gain a complete understanding of the structure of these decays; they are the simplest of B decays and also those with the largest exclusive branching ratios.

The first method for determining $|V_{cb}|$ begins with the inclusive branching ratio $\mathcal{B}_{SL} \equiv \mathcal{B}(B \to X_c\ell\nu)$. Combined with τ_B, this yields a partial width which can be compared to a theoretical expression. Naively, the semi-leptonic width, Γ_{SL}, is simply determined by the decay of a free b quark, akin to muon decay: $\Gamma_{SL} \sim |V_{cb}|^2 m_b^5$.

There are some subtleties to contend with, however. First, what does one insert into the formula for m_b? This involves issues of quarks vs hadrons and "duality." Furthermore, the rate superficially behaves as m_b^5 and is thus quite sensitive to the value used. Much theoretical work has been done attempting to clarify these issues. Another potential concern is that the LEP and CLEO results on the inclusive semi-leptonic rate historically have hinted at disagreement. The largest background to the inclusive lepton spectrum comes from secondary $D \to X\ell\nu$ decays. By looking at both like- and unlike-sign lepton pairs in $B\bar{B}$ decays, one can separate the primary leptons from B decay and those leptons from D decay (after including a straightforward correction for B mixing). Such an analysis was performed on 3 fb^{-1} of CLEOII data. This dilepton analysis uses one stiff lepton, ℓ, as a tag to isolate $B\bar{B}$ events. Then, by looking at additional inclusive electrons and counting like- and unlike-sign ℓe pairs, one extracts the lepton spectra for both $b \to Xe\nu$ and $c \to Xe\nu$; the final result is displayed in Fig. 4. The numerical results are:[7]

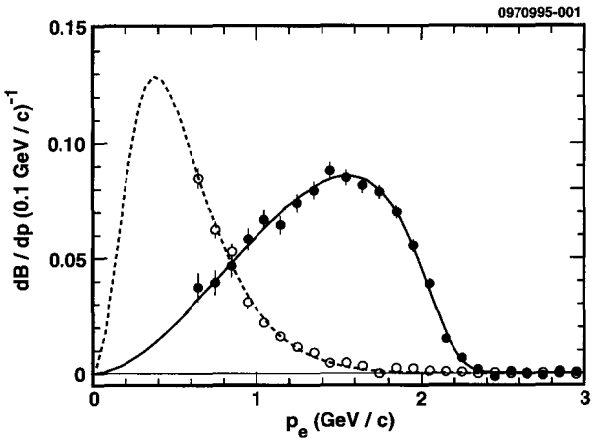

Fig. 4. Lepton momentum spectra derived from the dilepton analysis. Solid circles denote $B \to Xe\nu$; open circles, $D \to Xe\nu$.

$$\mathcal{B}(B \to Xe\nu) = 10.49 \pm 0.17(stat) \pm 0.43(syst)\%, \quad (10)$$

$$|V_{cb}| = 0.040 \pm 0.001(exp) \pm 0.004(theory). \quad (11)$$

The experimental error on this branching ratio is already quite small, so the limitation is currently theoretical. Some may feel that theoretical error on $|V_{cb}|$ is already better than 10%. CLEO is working to update this analysis with more data, and improved reconstruction and Monte Carlo. Some possibilities for aiding theorists with new measurements are also discussed below. Another technique for extracting $|V_{cb}|$ is found in the marriage of exclusive modes and HQET and involves measuring $d\Gamma/dq^2$ for $D^*\ell\nu$. Then, extrapolating in q^2 to zero recoil yields $|V_{cb}|\mathcal{F}(1)$, where $\mathcal{F}(1)$ is the form-factor at zero recoil ($w = 1$). Invoking HQET allows fairly accurate evaluations of $\mathcal{F}(1)$. Sensitivity to the shape of the form factor complicates this extrapolation. There are also

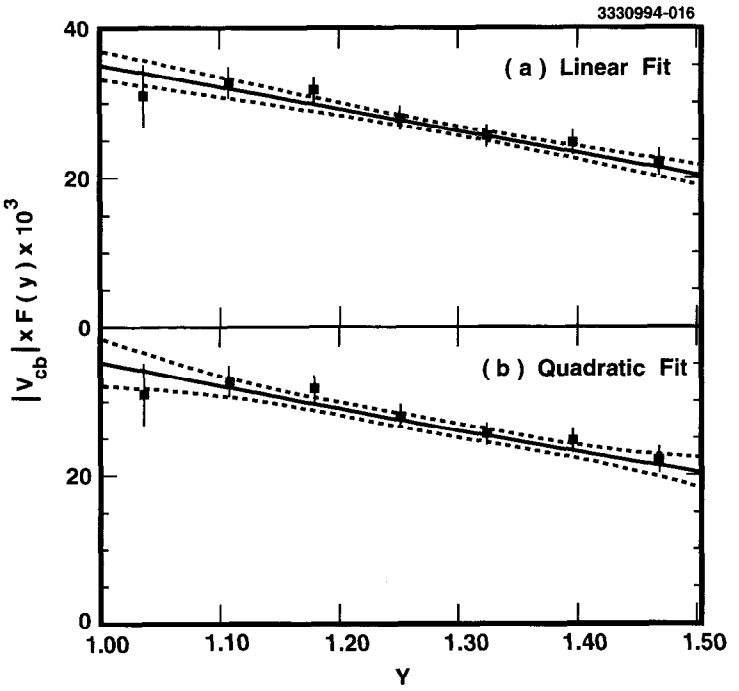

Fig. 5. Fits to the form-factor data for $D^*\ell\nu$ decays versus Y, which is essentially the HQET parameter w (see Ref. 8 for details). Both linear and quadratic fits are shown; in each, the solid line shows the central fit enclosed in the dashed error bands corresponding to one-sigma variations of the fit parameters. Error bars are statistical only.

corrections to the $m_Q = \infty$ limit of HQET; the mentioned earlier.

An analysis was performed on both the D^* CLEOII data. The use of both charge states a of charged and neutral B production fractions, and the extrapolation to zero-recoil, shown in

$$|V_{cb}|\mathcal{F}(1) = 0.0351 \pm 0.0019(stat)$$

A typical theoretical value for the form-factor

Finally, let us return to the method of det leptonic decay rate. The main problem invol level picture and the reality of hadronic bound s with help from the operator-product expansio new parameters. The OPE parameters are $\bar{\Lambda}$, (or 'brown muck'), λ_1, the kinetic energy of hyperfine chromo-magnetic interaction. The p perimental value of $m_{B^*} - m_B$. Further experi parameters $\bar{\Lambda}$ and λ_1, aiding theorists with inc quarks bound in B mesons.

In particular, CLEO is working to constrai ments of semi-leptonic decay variables. As a moment': it is just a sum over all events with ments, such as a mean or RMS, can constrain the lepton energy moments:

$$< E_\ell >, < (E_\ell -$$

are used, where E_ℓ is the lepton energy and $<$ These, along with corresponding hadronic ma which may be used to constrain theory.

Preliminary analyses are in progress to de moments.[9] They should provide accurate en them from being a serious source of error wh that even the $D^*\ell\nu$ HQET technique requires form factor at zero recoil and will also benefit.

The analysis obtaining the hadronic moments uses neutrino reconstruction on 5 fb^{-1} of CLEOII data. One can get the hadronic mass from just the measured ν and ℓ by taking the B to be at rest, and folding in the effects of the small motion as a correction. This avoids having to partition tracks and showers between the two overlapping B decays which would be necessary, and very difficult, to explicitly reconstruct the recoiling hadronic system. The leptonic moment analysis uses 3 fb^{-1}, employing the same dilepton technique as the inclusive branching ratio measurement described above. The lepton spectrum is cleanly determined down to 600 MeV/c; corrections for the small unseen tail are straightforward.

Given theoretical calculations for the moments in terms of $\bar{\Lambda}$ and λ_1, each experimental moment result constrains these parameters to lie in a band. The resulting constraints are displayed in Fig. 6. There is an apparent disagreement between the hadronic and leptonic constraints. It is not clear at this time how the blame is to be divided among statistics, measurement, and theoretical calculations. Since this method in principle promises very accurate results for $|V_{cb}|$, much effort is being expended to clarify the situation.

4.4 Outlook for $|V_{ub}|$ and $|V_{cb}|$

The $b \to u$ neutrino reconstruction analysis will focus on the q^2 dependence next; three times more data than used for the published results will soon be available. There remains one crucial need from theory: the absolute normalization of the form-factor, at *any* q^2 value, in order to tie the exclusive measurement to $|V_{ub}|$. Novel techniques may allow even lattice calculations to help out, despite the low-mass mesons.

An improved determination of $|V_{cb}|$ from the full reconstruction of $D^*\ell\nu$ events is also in progress. More data is available to study the form-factor curvature. The $D^{*+} - D^0$ mass difference resolution is now improved, reducing background in both old and new data. There is also a large effort to better understand the slow pion efficiency in order to reduce that source of systematic error. CLEO will also update the inclusive branching ratio while trying to resolve the issues involved in using the moment measurements to constrain the OPE parameters.

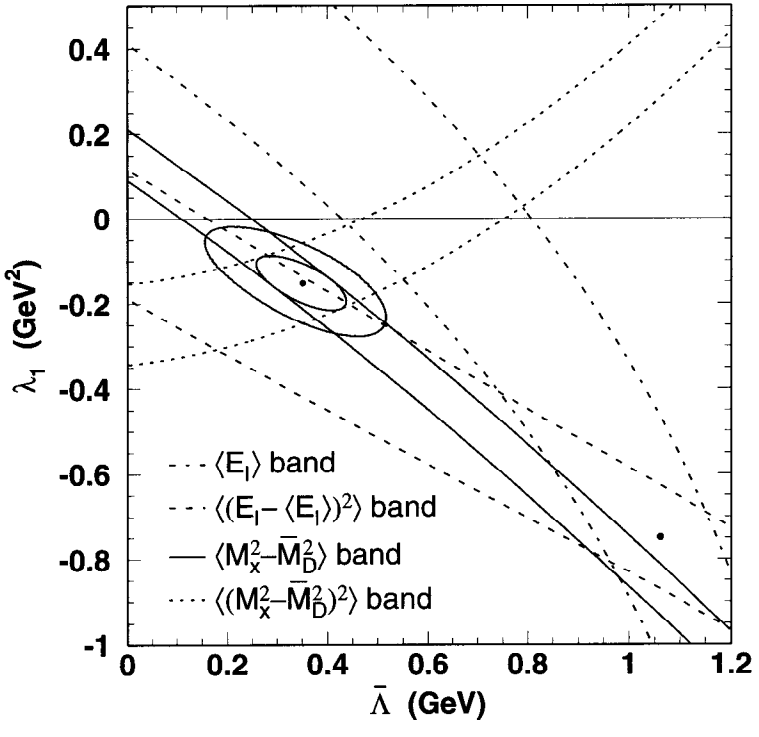

Fig. 6. Preliminary results on constraints from the four measured hadronic and leptonic moments are shown in the $\lambda_1 - \bar{\Lambda}$ plane. Two dots show the central solutions for the hadronic and leptonic moments separately. For the hadronic bands, $1, 2\sigma$ error ellipses are shown surrounding the central intersection point.

5 Rare Decays and CP-Violation

We now turn from the magnitudes of the CKM matrix elements to their phases. So far, CP violation has only been observed in neutral kaon decay. The one free phase parameter in the standard CKM matrix may be the sole source of this effect, but confirmation of model predictions in B physics is needed to provide the required independent test. The key modes include rare charmless decays as well as Cabibbo-suppressed decays to final states with charm. Some of the Feynman diagrams responsible for the rare charmless B decays are shown in Fig. 7. CP-violation can be observed in various ways. One

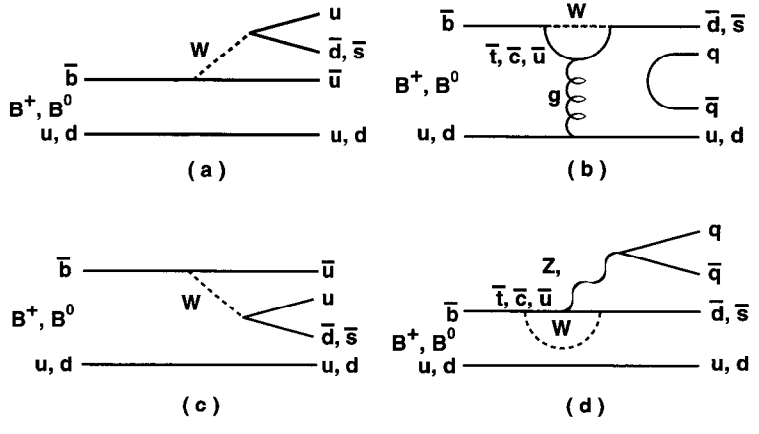

Fig. 7. Important Feynman diagrams responsible for rare charmless B decays: (a) external (color-allowed) spectator, (b) gluonic penguin, (c) internal (color-suppressed) spectator, and (d) electroweak penguin.

popular theme involves looking at time-dependent asymmetries in the decay rate to a CP-eigenstate, f_{CP}. Here, one utilizes mixing to interfere the decay paths $B \to f_{CP}$ and $B \to \bar{B} \to f_{CP}$ measuring, in the Standard Model, the phase of V_{td} present in the mixing process. CP-violation may also show itself via rate asymmetries between B and $\bar{B}$ decays to a final state f and its conjugate $\bar{f}$, respectively. These rate asymmetries require two interfering diagrams with a relative weak phase as well as a strong phase from final state interactions (FSI). The weak phase may come, for example, from the phase of V_{ub} in the spectator diagram relative to the gluonic penguin.

Many papers have analyzed the various decays and suggested ways of isolating the interesting information. CLEO is now cataloging many of the interesting final states and is usually observing them for the first time. Of key importance is the relative size of certain classes of diagrams, i.e., penguin and $b \to u$ spectator processes.

As an example of one general feature, note that penguin processes easily produce kaons, since CKM factors favor $b \to s$ over $b \to d$, while $b \to u$ spectator diagrams favor pions, due to Cabibbo-suppression of $W^- \to \bar{u}s$ relative to $W^- \to \bar{u}d$. As summarized below, CLEO observes the K modes rather than the π modes, hinting that penguins are large. In fact, $B^0 \to \pi^+\pi^-$ is not yet observed. This will make planned CP studies using this channel perhaps more difficult than originally suspected.

5.1 Rare Cabibbo-Suppressed $b \to c$ Decays

Let's begin with a Cabibbo-suppressed decay which is related to the well-established Cabibbo-allowed decay $B^0 \to D_s^+ D^{*-}$. The decay $B \to D^{*+}D^{*-}$ is of interest for time-dependent CP-violation studies, just like those planned for $\psi K^{(*)}$. One will have to determine the CP-content of the final state, as CLEO did for ψK^*,[10] in order to make real use of this mode.

The analysis is a standard full reconstruction of the entire B decay, using 8.5 fb^{-1} of CLEOII data. One noteworthy cut examines the significance of the vertex separation between the two Ds; this works particularly well with the subset of data (about 40%) taken with the SVX detector in place.

The final ΔE-M_B plot shows a clear excess in the signal region; see Fig. 8. The background is estimated in several ways, almost exclusively based on clever uses of the data, to be 0.31 ± 0.10. The probability that the four candidate signal events arise from a background fluctuation is estimated as 1.1×10^{-4}. This first observation yields the preliminary branching ratio:[11]

$$\mathcal{B}(B^0 \to D^{*+}D^{*-}) = (6.2^{+4.0}_{-2.9} \pm 1.0) \times 10^{-4} \qquad (14)$$

consistent with the Cabibbo-suppression, and other simple factors, relative to $D_s^* D^{*-}$.

CLEO also has another recent observation of a Cabibbo-suppressed decay of interest for CP-violation studies, $B^- \to D^0 K^-$, with 5 fb^{-1} of CLEOII data:[12]

$$\mathcal{B}(B^- \to D^0 K^-) = (2.57 \pm 0.65 \pm 0.32) \times 10^{-4}. \qquad (15)$$

Current analyses are working on other Cabibbo-suppressed modes such as $D^{*+}D^-$, D^+D^-, and D^0K^{*-}.

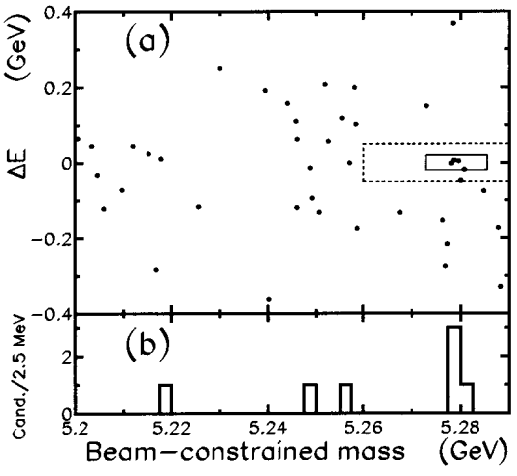

Fig. 8. The ΔE vs M_B distribution for the $B \to D^{*+}D^{*-}$ candidates. The solid box is the signal region; the sideband outside the dashed box is used to help evaluate background levels. Shown below is the mass projection with the ΔE cut used for signal.

5.2 Angular Analysis of $B \to D^*\rho$ and Search for FSI

Final state interactions are required in order for inclusive decay-rate asymmetries to be non-zero. It is sometimes argued that in decays such as $B \to K\pi$, the decay products separate so fast that such phases must be small, but the truth is far from clear. Given this, it is interesting to look for evidence of FSI phases anywhere in B physics. In B decays to charm, perhaps the slower relative motion of the decay products will admit an observable effect.

A new analysis examines the $D^*\rho$ final state; it has relatively good statistics, and a non-trivial angular distribution. This is the first full fit to this angular distribution; previously, CLEO has done a similar analysis of ψK^* decays.[10]

A maximum likelihood fit to three helicity amplitudes, H_+, H_-, H_0, is performed. Factorization can be checked by comparing $\Gamma_L/\Gamma = |H_0|^2/\sum|H_i|^2$ with Γ_L/Γ for $B \to D^*\ell\nu$ at $q^2 = m_\rho^2$. Finally, one can look for hints of final state interactions in the relative phases of the H_i. The analysis uses 5 fb^{-1} of CLEOII data. The preliminary

$B^0 \to D^{*-}\rho^+$	magnitude
H_0	0.936
H_-	$0.317 \pm 0.052 \pm 03$ (
H_+	$0.152 \pm 0.058 \pm 07$]
$B^+ \to \bar{D}^{*0}\rho^+$	magnitude
H_0	0.932
H_-	$0.283 \pm 0.068 \pm 09$]
H_+	$0.228 \pm 0.069 \pm 06$ (

Table 1. Preliminary results of the fit to thelicit
The phase of H_0 is zero by convention and thmpli
$\sum|H_i|^2 = 1$.

result for Γ_L/Γ, along with some relevant compsons

$D^{*-}\rho^+$: $\Gamma_L/\Gamma = 0.8 \pm 0.$
CLEO $D^*\ell\nu$: $\Gamma_L/\Gamma = 0.9 \pm 0.$
Theory : $\Gamma_L/\Gamma \simeq 0.8$- 0.8

Table 1 summarizes the preliminary results of tletai

Factorization appears to be working, withine er the phases, but they are not yet significant bason tl phases are fixed at zero. It is possible to look fonases angular terms with $Im(H)$ explicit in them, bthis current statistics. Work is in progress to add mcdata

5.3 Analysis of Rare Charmless B Eays

Let us now turn to the rare charmless B decays.:fore is useful to briefly discuss some common aspeof the

First, in order to keep efficiencies as high asssibl fits to extract yields. These fits include quantitisuch and helicities, particle ID information, shape vaoles

When plotting M_B, for example, to illustrate resu other variables beyond those used to select eveifor t

to see sidebands. Thus, the full statistical power of the data is not evident in these fit projections. The likelihood results are also cross-checked with simple cut-and-count analyses, looking at events above background in a ΔE-M_B signal box after all cuts.

Due to our limited ability to separate the stiff charged Ks and πs produced in two-body charmless B decays, simultaneous fits are used. For example, the rates for $B^+ \to \eta' K^+$ and $B^+ \to \eta' \pi^+$ are extracted from one fit. In such cases, the likelihood contours as a function of the two yields (or branching ratios) are displayed. The K-π separation at 2.6 GeV/c from dE/dx is about 2σ and an additional, independent 1.7σ is obtained from the mass-dependence inherent in calculating ΔE. The notation h is sometimes used to denote an undifferentiated combination of charged πs and Ks.

CLEO recently published three major papers, all based on 5 fb^{-1} of CLEOII data. These publications covered $K\pi$ and related final states,[14] final states with an η or η',[15] and final states containing an ω or ϕ.[16] These results are summarized graphically in Figs. 9 and 10. A few peculiar* modes from the three publications are omitted from these graphics. Some other modes are shown which have not been updated recently; these results are contained in an earlier paper.[17]

Now we summarize the recent, unpublished updates to these results.

5.4 Recent Updates for Rare Charmless B Decays

A preliminary update of modes with η''s was given at ICHEP98.[18] The analyses were performed with 8.5 fb^{-1} of CLEOII data. As discussed earlier, the $\eta' K^+$ and $\eta' \pi^+$ modes are fit simultaneously; the resultant likelihood contours for $\eta' h^+$ are shown in Fig. 11. The data indicates only K^+ in the final state, with no hint of π^+ yet. Figure 12 shows ΔE and M_B projections for these $\eta' h^+$ final states as well as for $\eta' K_S$. These new η' results are summarized in Table 2.

ICHEP98 further witnessed a preliminary update of $B^0 \to K^+\pi^-$ and related modes also using 8.5 fb^{-1} of data.[19] Figure 13 shows the likelihood contours for the $K^+\pi^-$ and $\pi^+\pi^-$ yields, and displays the clear evidence for a signal in the key projection plots. The yields for $K^+\pi^-$, $\pi^+\pi^-$ are extracted simultaneously, and only $K^+\pi^-$ is significant. This is a sign that penguins are large. Also, the contours in Fig. 13 indicate that it is unlikely for the $K^+\pi^-$ and $\pi^+\pi^-$ modes to have equal branching ratios.

Analogous plots for $h^\pm K_S$ and $h^\pm \pi^0$ modes are shown in Figs. 14 and 15. The new

*These are $\phi\pi$, $\phi\rho$, $\phi\omega$, and $\phi\eta^{(\prime)}$. All have an $s\bar{s}$ in the final state and are not easily accessible via W-emission or penguin diagrams and so are expected to have very small branching ratios.

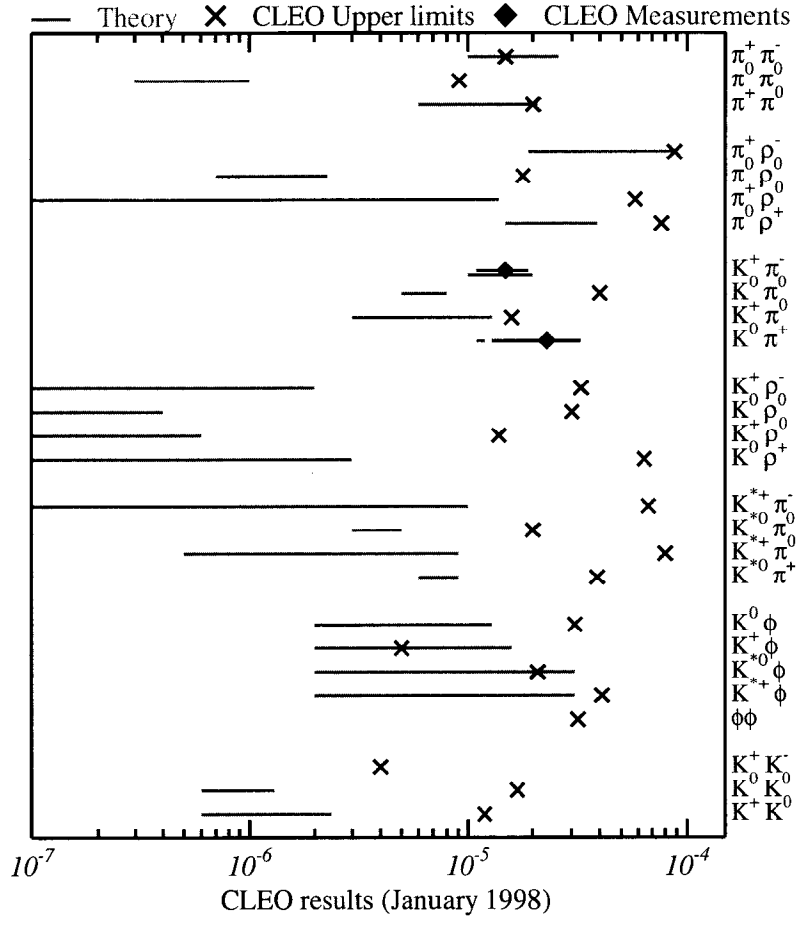

Fig. 9. A graphical summary of *published* CLEO rare charmless B decay results. All results are based on 5 fb^{-1} of CLEOII data, except modes of the form $h\rho$ and $K^*\pi$, which use 3.6 fb^{-1}. Note that some updated conference results are presented later, including the first observation of $B^+ \to K^+\pi^0$.

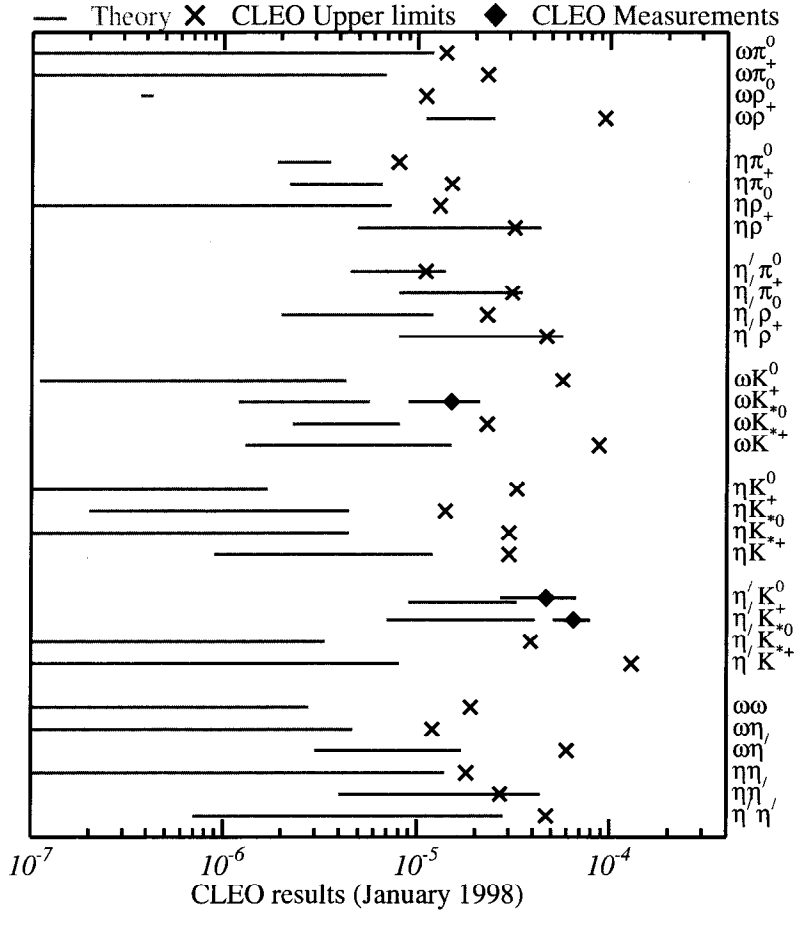

Fig. 10. A graphical summary of *published* CLEO rare charmless B decay results. All results are based on 5 fb^{-1} of CLEOII data. Note that some updated conference results are presented later.

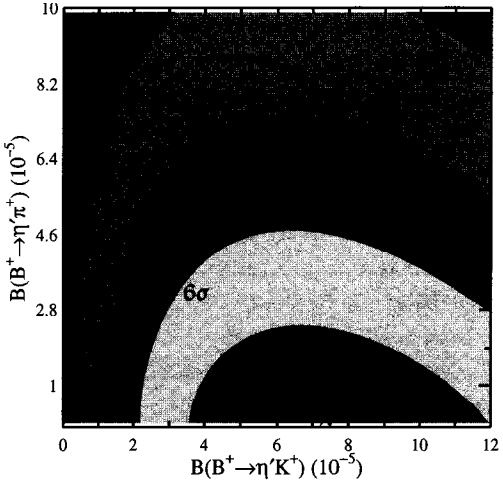

Fig. 11. Contours from the likelihood fit for the $B \to \eta' K^+$ and $B \to \eta' \pi^+$ branching ratios.

$KK, K\pi, \pi\pi$ results are summarized in Table 3; note that $B^+ \to K^+\pi^0$ is a new first observation.

Further updates on many modes, including more $B \to PV$ (pseudo-scalar vector) modes, like πK^* and $\pi\rho$, are expected to become available in the near future.

Mode	$\epsilon(\%)$	$N_{\rm signal}$	Signif.	$\mathcal{B}(\times 10^{-5})$
$\eta' K^+$	$29-36$	68.6	12.7	$7.4^{+0.8}_{-1.3} \pm 1.0$
$\eta' K^0$	$28-33$	16.1	7.3	$5.9^{+1.8}_{-1.6} \pm 0.9$
$\eta'\pi^+$	$29-36$	1.0	-	< 1.2

Table 2. A summary of new preliminary results for modes including an η'. Note that these results are NOT included in Figs. 9 and 10.

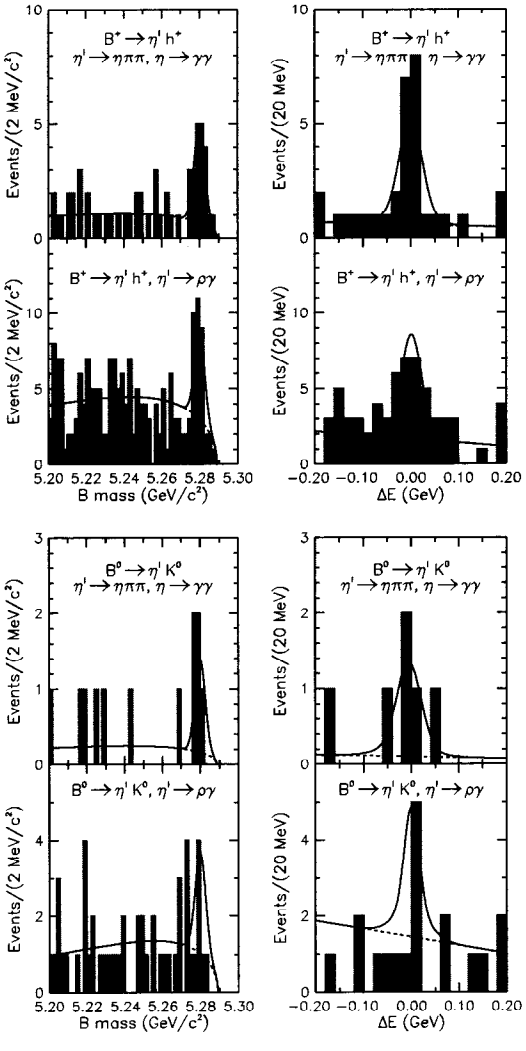

Fig. 12. Projections of ΔE and M_B for η' modes with an observed signal. The top four plots show projections for $\eta' h^{\pm}$ separated into two different η' decay channels; the bottom four plots are the analogous ones for $\eta' K_S$.

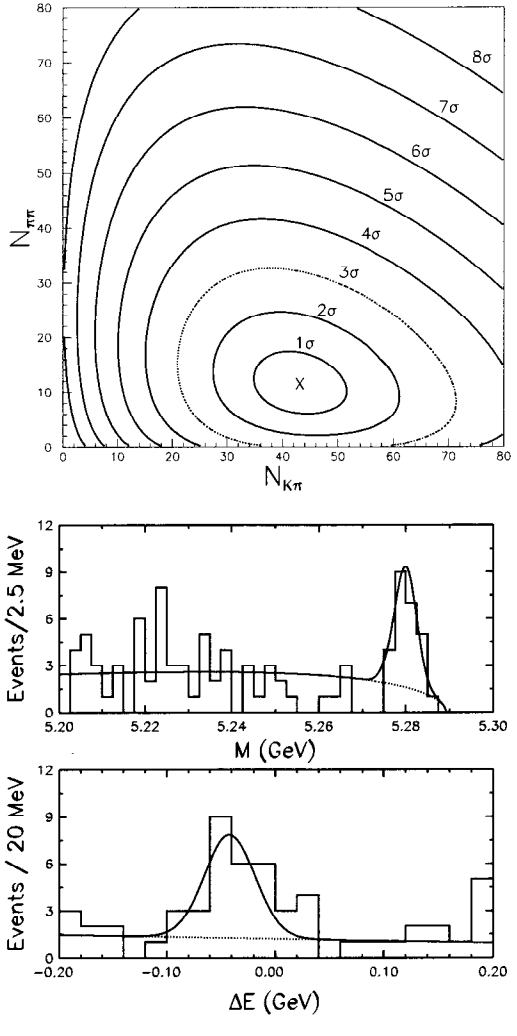

Fig. 13. The top plot shows the contours from the likelihood fit to $K^{\pm}\pi^{\mp}$ and $\pi^{\pm}\pi^{\mp}$ yields. The two lower plots are ΔE and M_B projections for the $h^{\pm}\pi^{\mp}$ signal. Note that our reconstruction assumes the π mass for all charged tracks, so ΔE shifts to -42 MeV for true $K^{\pm}\pi^{\mp}$.

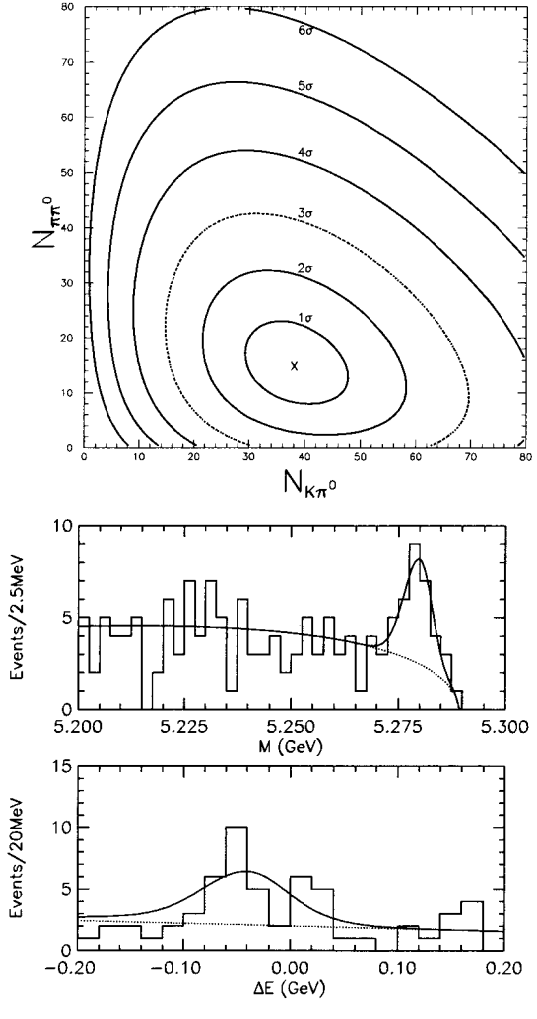

Fig. 14. The top plot shows the contours from the likelihood fit to $\pi^{\pm}\pi^0$ and $K^{\pm}\pi^0$ yields. The two lower plots are ΔE and M_B projections for the $h^{\pm}\pi^0$ signal. Note that our reconstruction assumes the π mass for all charged tracks, so ΔE shifts to -42 MeV for true $K^{\pm}\pi^0$.

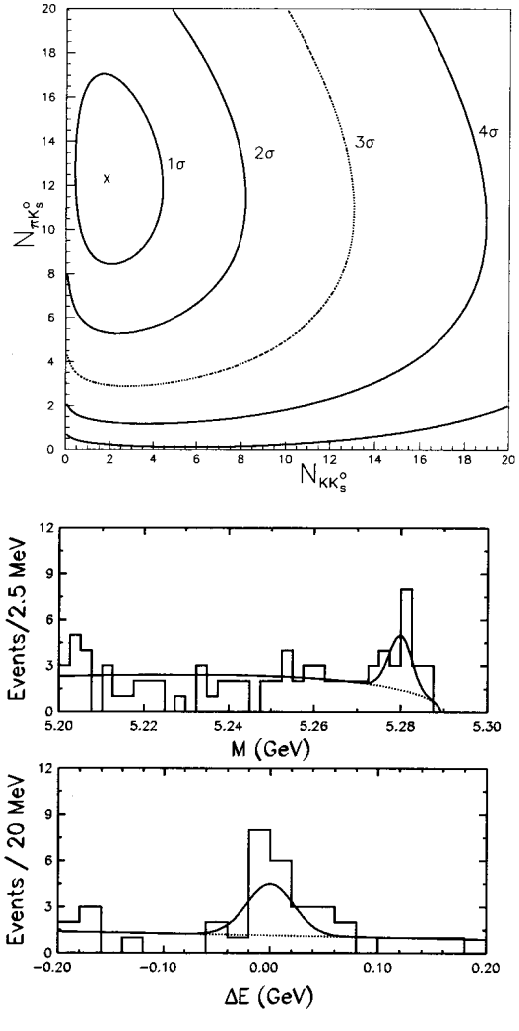

Fig. 15. The top plot shows the contours from the likelihood fit to the $\pi^{\pm}K_S$ and $K^{\pm}K_S$ yields. The lower plots are ΔE and M_B projections for the $h^{\pm}K_S$ signal.

Mode	$\mathcal{E}(\%)$	$\mathcal{B}$ (10^{-5})	Theory $\mathcal{B}$ (10^{-5})
$\pi^+\pi^-$	53 ± 5	< 0.84	0.8–2.6
$\pi^+\pi^0$	42 ± 4	< 1.6	0.4–2.0
$K^+\pi^-$	53 ± 5	$1.4 \pm 0.3 \pm 0.2$	0.7–2.4
$K^+\pi^0$	42 ± 4	$1.5 \pm 0.4 \pm 0.3$	0.3–1.3
$K^0\pi^+$	15 ± 2	$1.4 \pm 0.5 \pm 0.2$	0.8–1.5
K^+K^-	53 ± 5	< 0.24	–
$K^+\bar{K}^0$	15 ± 2	< 0.93	0.07–0.13

Table 3. A summary of new preliminary results for PP modes, where $P = \pi^\pm, \pi^0, K^\pm$, or K_S. Note that these results are NOT included in Figs. 9 and 10.

5.5 $B \to \eta_c K$

CLEO has observed large rates for the $B \to \eta' K$ decays. Some explanations for these rates have posited a $c\bar{c}$ component in the η'. This has motivated a search for the related $\eta_c K$ mode.

The analysis uses 5 fb^{-1} of CLEOII data in a maximum likelihood fit, just as is done for the charmless rare B decays. Only the $\eta_c \to \phi\phi$ decay is used; it has a small branching ratio ($\sim 0.7\%$), but is very clean. Figure 16 shows some of the kinematic distributions for the candidate events. There are two candidates with very low background; this gives a 3.9σ significance.

The preliminary result for the measured branching ratio is consistent with expectations based on the ψK rate:[20]

$$\mathcal{B}(B^- \to \eta_c K^-) = (1.54^{+1.39}_{-0.87}(stat) \pm 0.15(syst) \pm 0.60(\eta_c BR)) \times 10^{-3}. \quad (19)$$

Limits on some related modes are given in Table 4. Adding the $\eta_c \to K_S K\pi$ decay mode in the future will further increase our sensitivity.

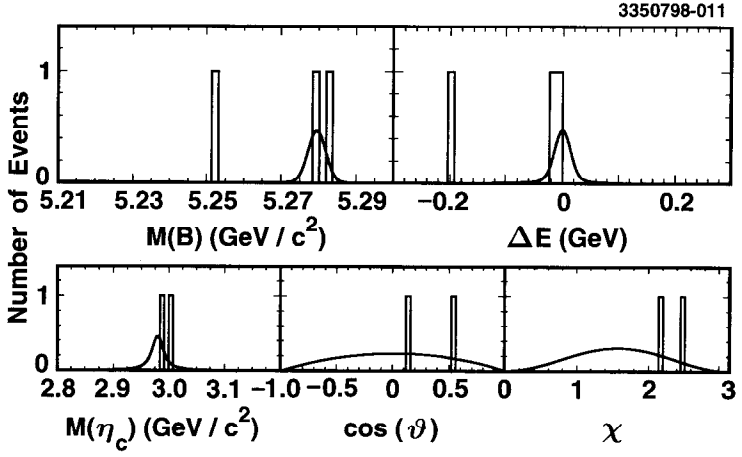

Fig. 16. The ΔE and M_B projections of the $\eta_c K^-$ fit. Also shown are the η_c mass, and the η_c decay angles.

Decay Channel	Upper Limit (90% C.L.)
$B^0 \to \eta_c K^0$	6.8×10^{-3}
$B^0 \to \eta_c K^{*0}$	5.95×10^{-3}
$B^\pm \to \eta_c K^{*\pm}$	18.5×10^{-3}

Table 4. Preliminary upper limits for modes related to the $B^- \to \eta_c K^-$ signal.

6 Rare Decays from Electroweak Penguins

Decays mediated by electroweak penguins are of considerable interest. The inclusive rate for $b \to s\gamma$ was first measured by CLEO.[21] It is a very important constraint on physics beyond the Standard Model; for example, it may be used to constrain the charged Higgs in SUSY models. This analysis has recently been updated.

The largest backgrounds come from $q\bar{q}$ continuum processes and initial-state radiation. It is difficult for generic B decays to make photons as stiff as those in the signal process. CLEO's analysis uses two techniques which are combined for the final result; only a brief summary of the techniques is given here.

Method one is a "shape analysis" which looks for only the stiff photon. A sophisticated combination of variables, including event shape and energy flow, is used to suppress background. The end result is an event weight which characterizes the chance that a given event is signal or background.

Method two utilizes a modified full reconstruction. A stiff photon, a kaon ($K^{\pm}$ or K_S), and from zero to four pions (where at most one π is a π^0) are combined in search of a viable B candidate. For each event, the best such candidate is picked based on a grand χ^2 which includes ΔE, M_B, particle ID information, and any K_S or π^0 masses. Finally, an event weight is produced as in method one; it is a function of ΔE, M_B, and $cos\theta_{tt}$ (where θ_{tt} is the angle between the candidate B thrust axis and the rest of the event).

A combined event weight is calculated when an event is present in both methods; the reconstruction analysis events are a subset of the shape analysis events. This technique yields greater statistical power than our previous, published analysis. More data and a lower photon energy cut (2.1 vs 2.2 GeV) are also used for this update. The measured E_γ spectrum is detailed in Fig. 17, showing a clear excess in the energy range expected from a quasi-two body γX_s final state. Our new preliminary result based on 5 fb^{-1} is:[22]

$$\mathcal{B}(b \to s\gamma) = (3.15 \pm 0.35(stat) \pm 0.32(syst) \pm 0.26(model)) \times 10^{-4}. \quad (20)$$

This is consistent with our old result and also very consistent with theory:[23]

$$\mathcal{B}(b \to s\gamma) = (3.28 \pm 0.33) \times 10^{-4}. \quad (21)$$

There are many related electroweak penguin modes also under study. The $B \to K^*\gamma$ decay was discovered by CLEO,[24] however $B \to \rho\gamma$ has yet to be seen. The ratio of branching fractions for these two modes can give $|V_{td}/V_{ts}|$. The latest results[25] use only 3.5 fb^{-1} of data; work on an update is underway.

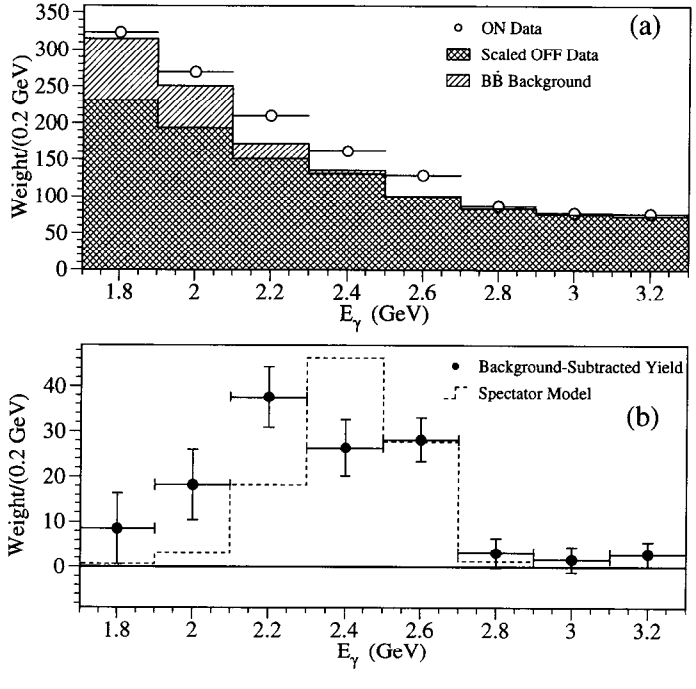

Fig. 17. The observed E_γ spectrum from the $b \to s\gamma$ analysis is shown in (a). The dominant background is from continuum events, but $B\bar{B}$ events come into play at lower photon energies. The background-subtracted plot in (b) shows a clear excess which is compared to a simple hadronization model shown as the dashed histogram.

Modes where the photon materializes as a lepton pair are sensitive to more terms in the effective Hamiltonian than $b \to s\gamma$ itself and thus are of interest also. Both an inclusive $b \to s\ell^+\ell^-$ and an exclusive $B \to K^{(*)}\ell^+\ell^-$ analysis have been performed with 5 fb^{-1} of CLEOII data. The inclusive results are:[26]

$$\mathcal{B}(b \to s\, e^+e^-) < 5.7 \times 10^{-5}, \quad (22)$$

$$\mathcal{B}(b \to s\, \mu^+\mu^-) < 5.8 \times 10^{-5}, \quad (23)$$

$$\mathcal{B}(b \to s\, e^\pm\mu^\mp) < 2.2 \times 10^{-5}, \quad (24)$$

$$(25)$$

while the preliminary exclusive results are:[27]

$$\mathcal{B}(B \to K^*\ell^+\ell^-) < 0.68 \times 10^{-5}, \quad (26)$$

$$\mathcal{B}(B \to K\ell^+\ell^-) < 0.70 \times 10^{-5}. \quad (27)$$

All are 90% C.L. limits.

Both the inclusive and exclusive dilepton modes have sensitivities which are approaching the theoretical expectations. Perhaps some of these modes, and the exclusive $\rho\gamma$ final state, will be seen in the next round of B experiments, providing us with further insights and constraints.

7 *D* Lifetimes with the Silicon Vertex Detector

CLEO now has the opportunity to make precise measurements of charm meson and baryon lifetimes due to the excellent resolution of the new silicon vertex detector. The first such analysis to explore these possibilities uses 3.7 fb^{-1} of CLEOII.V data and measures the D meson lifetimes.

The charm mesons were reconstructed via the following decay modes:

$$D^0 \to K^-\pi^+, \quad K^-\pi^+\pi^0, \quad K^-\pi^-\pi^+\pi^+, \quad (28)$$

$$D^+ \to K^-\pi^+\pi^+, \quad (29)$$

$$D_s \to \phi\pi^+ \quad (\text{with } \phi \to K^+K^-). \quad (30)$$

For the D^0 (D^+), a slow π^+ (π^0) was required to form a good $D^{*+} \to D^0\pi^+$ ($D^{*+} \to D^+\pi^0$) candidate in order to reduce background. No tagging was required for the D_s mesons.

The D flight path is extrapolated to the flat, well-known beam spot to determine the production point. The beam spot size is given by $\sigma_y \sim 7\,\mu$m, $\sigma_x \sim 350\,\mu$m, and is determined on a run-by-run basis. This construction is illustrated in Fig. 18. Fragmentation tracks, which may bias the interaction point, are avoided. The $D^0 \to K^-\pi^+$ vertex resolution varies from about 60–110 μm, along the flight direction, compared to a typical flight of $< \gamma\beta c\tau > = 200\mu$m. Only the two-dimensional projection of the decay in the $r - \phi$ plane is used. This is done by choice; the silicon z measurements are available if desired.

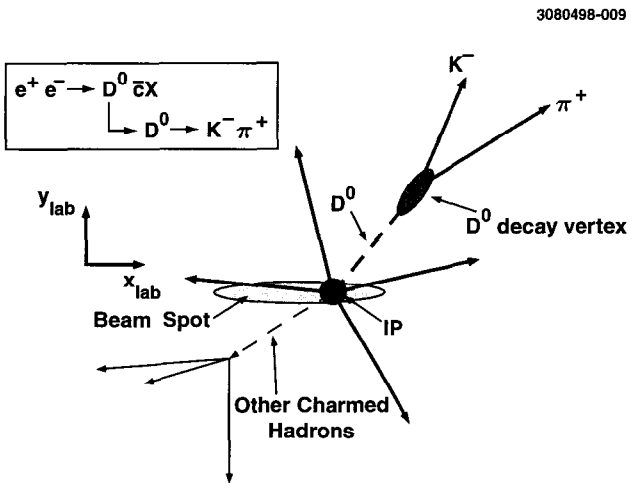

Fig. 18. An illustration of the technique used in determining charm lifetimes; see the text for further description.

An unbinned maximum-likelihood fit with seven parameters is used to extract results. The fit parameters are: the D lifetime, the fraction of background with lifetime, the lifetime of this background, the fraction of mis-reconstructed events and their average resolution, the fraction of "flat" background (with a fixed resolution of 6 ps), and a scale factor for the predicted measurement error (found to be 1.13 ± 0.02). Figure 19 shows the fit to the proper lifetime data.

The preliminary results for the lifetimes of the D^0, D^+, and D_s^+ mesons are:[28]

$$D^0 \;:\; 408.5(stat) \pm 4.1^{+3.0}_{-2.9}(syst) \text{ fs}, \quad (31)$$

$$D^+ \;:\; 1033.6(stat) \pm 22.1^{+7.4}_{-10.9}(syst) \text{ fs}, \tag{32}$$

$$D_s \;:\; 486.3(stat) \pm 15.0^{+3.8}_{-4.0}(syst) \text{ fs}. \tag{33}$$

The D^0 lifetime reported here is comparable in precision with the world average and the D_s lifetime is more precise than the world average. The excellent $D^* - D$ mass-difference resolution in the CLEOII.V data is illustrated in Fig. 20; the resolution is 210 KeV. This is achieved with a three-dimensional vertex fit to improve the slow-pion parameters. This resolution directly improves the signal to noise in certain key analyses. In particular, CLEO is re-measuring the doubly-Cabibbo-suppressed decay (DCSD) $D^0 \to K^+\pi^-$, first seen by CLEO.[29] With the silicon detector, CLEO will also be able to directly separate the DCSD process from possible $D - \bar{D}$ mixing, which is negligible in the Standard Model. Such excellent mass-difference resolution also begs for a study of the intrinsic width of the D^*, which may be directly accessible for the first time. Clean signals are also available for several D^0 decays to CP-eigenstates; preliminary peaks with loose cuts are shown in Fig. 20. More data and further background suppression are in hand already. These modes will be used to look for lifetime differences between the two CP-eigenstates of the D^0. Finally, efforts are underway to use the silicon for measuring charm baryon lifetimes.

8 Charm Baryons

Charm baryon spectroscopy is an area in which CLEO has recently displayed great prowess. Eight new states have been discovered since the 1996 PDG listing, all of them at CLEO. The newest among these are the two Ξ_c' states,[30] shown in Fig. 21, and the first two $L = 1$ Ξ_c states,[31] shown in Fig. 22. All these preliminary results use 5 fb^{-1} of data. In each case, the observation of the two expected charge states greatly aids our confidence in the existence and interpretation of these new states.

The world knowledge of charm baryon spectroscopy is summarized in Table 5. In addition to the ground state multiplets only the established $L = 1$ excitations are listed. CLEO has discovered 11 states, all other experiments combined have found six, and there are two $L = 0$ states (and likely many more narrow $L = 1$) states still to be found.†

†One might argue that the accounting is 10 and 7, rather than 11 and 6, if a single candidate Σ_c^+ is taken as a convincing discovery.

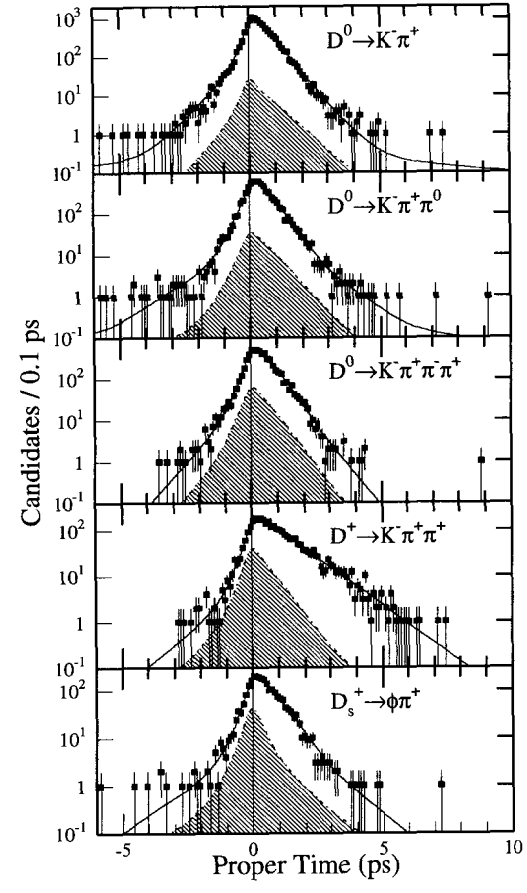

Fig. 19. The results of the D lifetime fits for each decay channel, shown as solid curves overlaid on the data points. The shaded histograms indicate the background level and shape.

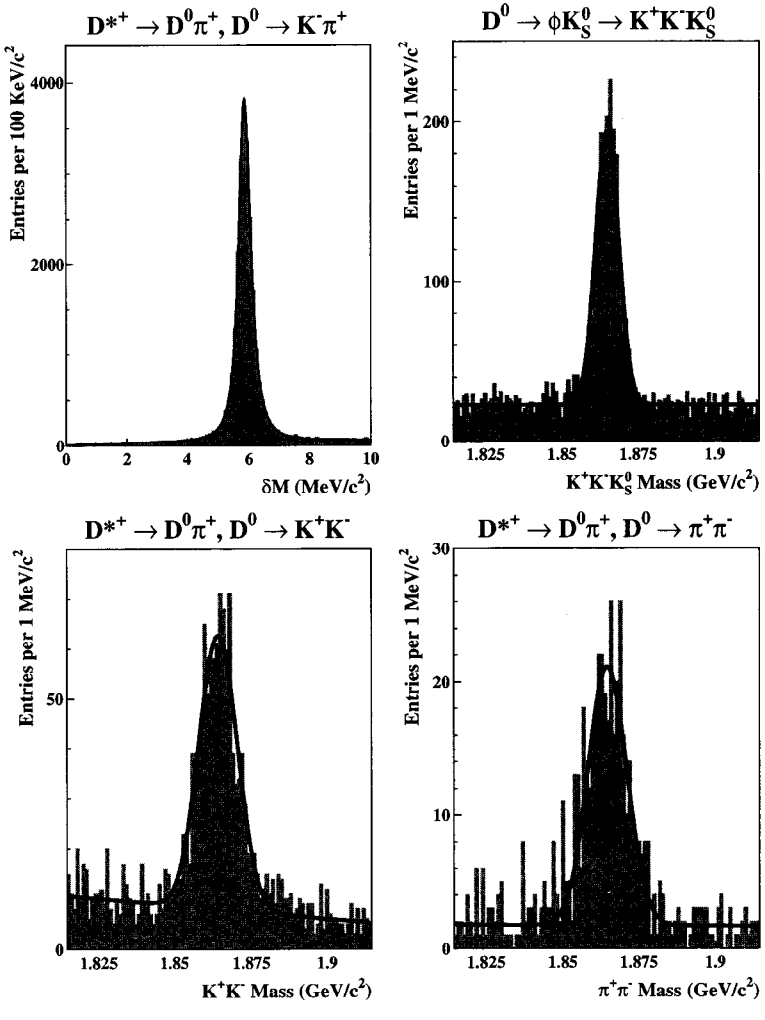

Fig. 20. The first plot demonstrates our excellent $D^* - D$ mass difference resolution; mass($K\pi\pi$) - mass($K\pi$) - m_π is plotted. The remaining plots show mass peaks for some decay modes of the D^0 into CP-eigenstates.

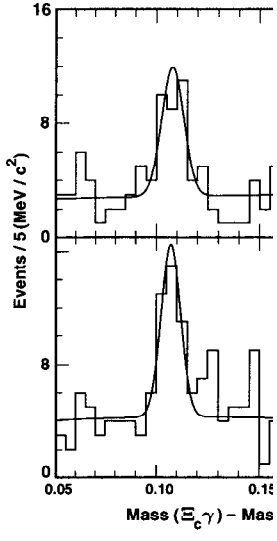

Fig. 21. Plots of the $\Xi_c\gamma - \Xi_c$ mass f

CLEO hopes to find even more narrow L : be increasingly careful when hunting for new ous correlated soft πs and γs from transitions underway working to catalog new decay mode as well.

In the near future, CLEO will measure cl vertex detector. An inclusive single-experim service. Finally, one crucial need in this field is $pK\pi$). Attempts are underway to contribute he

9 Tau Physics

CLEO has the world's highest statistics tau sa topics. The particular analysis discussed here a light hadron physics.

$L=0$ $J^P=1/2^+$			Ξ_c^0	Ξ_c^+	Ω_c^0	
			$\Xi_c^{0\prime}$	$\Xi_c^{+\prime}$		
	Λ_c^+		Σ_c^0	Σ_c^+	Σ_c^{++}	
$L=0$ $J^P=3/2^+$				Ω_c^{0*}		
			Ξ_c^{*0}	Ξ_c^{*+}		
			Σ_c^{*0}	Σ_c^{*+}	Σ_c^{*++}	
$L=1$ $J^P=1/2^+$	$\Lambda_c(2593)$					
$L=1$ $J^P=3/2^+$	$\Lambda_c(2625)$ $\Xi_c^+(2815)$ $\Xi_c^0(2820)$					

Table 5. A graphic illustration of CLEO's contributions to charm baryon spectroscopy. The top two sections are arranged according to $SU(3)$ multiplets. States underlined were first observed by CLEO. States not underlined were first seen by other experiments. States underlined twice are not yet established. Only the observed, narrow $L=1$ states are listed; the J^P assignments for many of the states are educated guesses.

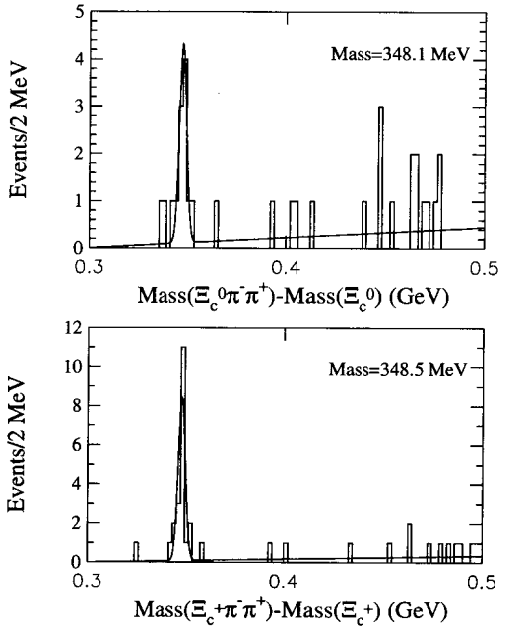

Fig. 22. Plots of the $\Xi_c\pi^-\pi^+ - \Xi_c$ mass for the $L=1$ Ξ_{c1}^0 and Ξ_{c1}^+ candidates.

A very thorough analysis of $\tau \to \pi^0\pi^0\pi^-$ was performed on 5 fb^{-1} of CLEOII data.[32] The decay is dominated by the s-wave $a_1(1260) \to \rho\pi$ component. Details of the $a_1(1260)$ state are poorly understood and tau decay is a perfect laboratory in which to study it. Recall also that the hadronic mass shape near the endpoint of the 3π mode is of interest for neutrino mass limit analyses.

The $\pi^-\pi^0\pi^0$ final state is superior to the $\pi^+\pi^+\pi^-$ one since it has lower hadronic and tau feed-across background. Also, there is only one $I=0$ combination of πs, making it ideal for looking at scalar resonances in the decay substructure.

The 3π Dalitz plots are fit for several components relative to the dominant s-wave $\rho\pi$ term. When this is done in bins of 3π mass, it is found that the data is well-described with resonance parameters which are independent of this mass; therefore we take these parameters as constant. A portion of the information extracted about the complex couplings for each channel is summarized in Table 6; more information is contained in the conference paper.[32]

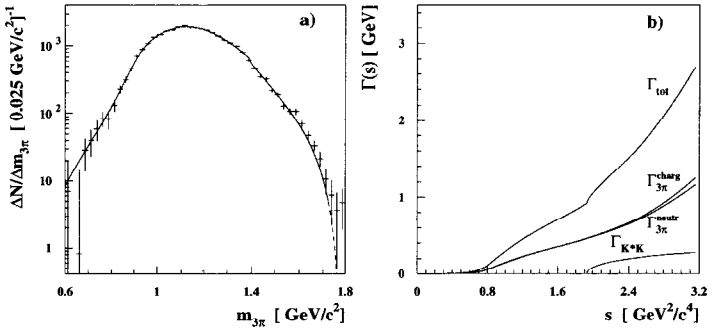

Fig. 23. The left plot shows the fit to the 3π invariant mass from $\tau \to \pi^0\pi^0\pi^-$ decays. On the right are the mass-dependent channel widths corresponding to this fit.

With the substructure determined, one can examine the 3π mass spectrum itself, which is dominated by the a_1 lineshape. The preliminary fit is shown in Fig. 23. Note that the high-mass structure visible there is partly from the K^*K threshold, which must of course be present. The coupling to this channel is allowed to float in the fit, with the turn-on shape taken from theory.

Resonance	L	Signif.	$\mathcal{B}$ fraction(%)
$\rho(1450)$	s-wave	1.4σ	$0.30 \pm 0.64 \pm 0.17$
ρ	d-wave	5.0σ	$0.36 \pm 0.17 \pm 0.06$
$\rho(1450)$	d-wave	3.1σ	$0.43 \pm 0.28 \pm 0.06$
$f_2(1275)$	p-wave	4.2σ	$0.14 \pm 0.06 \pm 0.02$
σ	p-wave	8.2σ	$16.18 \pm 3.85 \pm 1.28$
$f_0(1370)$	p-wave	5.4σ	$4.29 \pm 2.29 \pm 0.73$

Table 6. Results from preliminary fits to the substructure in the 3π system in $\tau \to \pi^0\pi^0\pi^-$ decays. The strength and significance of each component is noted. Note that the branching ratios do not sum to one due to interference.

This analysis also yields signed neutrino helicity via a decay asymmetry due to interference between the two $\pi^-\pi^0$ combinations present. The analysis yields $h_{\nu_\tau} = -1.02 \pm 0.13 \pm 0.03$, as compared to the expectation of -1.

A corresponding analysis looking at the $\pi^+\pi^-\pi^-$ mode has already produced some promising results.[32] Using the $\pi^-\pi^0\pi^0$ fit results in an appropriately modified current suitable for the $\pi^+\pi^-\pi^-$ final state, once can generate a Monte Carlo event sample. The agreement with the $\pi^+\pi^-\pi^-$ data is excellent, indicating that consistent results will be extracted from the two modes.

10 Two-Photon Physics

CLEO also makes good use of the two-photon physics reach in our dataset. One recent study involves determining the two-photon coupling of a glueball candidate.

From previous measurements of $\psi \to gg\gamma \to X\gamma$ done elsewhere, one can extract information on the coupling of a state X to gluons. Searching for X in two-photon production can measure or limit the coupling to $\gamma\gamma$.

One can then define for particle X a "stickiness," S:

$$S \sim \Gamma(\psi \to \gamma X)/\Gamma(X \to \gamma\gamma) \tag{34}$$

where the factors omitted compensate for effects of differing coupling constants, phase space and spins. Note that the branching ratio of X to the detected final state can be canceled. The value of S should be of $\mathcal{O}(1)$ for $q\bar{q}$ mesons, since valence quarks couple well to both glue and photons. CLEO has looked for two-photon production of the $f_J(2220)$ in both the K_SK_S and $\pi^+\pi^-$ final states. The invariant mass spectra of the candidates is shown for both searches in Fig. 24; in both cases, limits were extracted. The final combined result for the stickiness, S, is:[33,34]

$$S(f_J(2220)) > 102 \qquad 95\% \text{ C.L.}, \tag{35}$$

making the $f_J(2220)$ the stickiest state yet evaluated and strengthening the case for its interpretation as a glueball. One potential out would be to question the very existence of this state; although it has been seen by several experiments in several decay modes, some questions still remain.[35]

11 Other Recent Analysis Topics

There are many new summer conference papers which were not discussed, due to length constraints. These include:

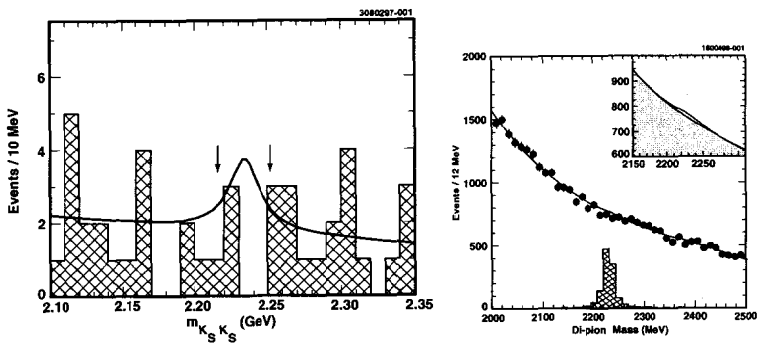

Fig. 24. The $K_S K_S$ (left) and $\pi\pi$ (right) invariant mass spectrum from searches for two-photon production of the $f_J(2220)$.

***B* Physics:**

- Observation of High Momentum η' Production in B Decay
- Search for $B \to \rho^0 K^0$, $B \to K^{*\pm}\pi^{\mp}$
- Distribution in q^2 of the Decay $\bar{B}^0 \to D^{*+}\ell\bar{\nu}$ via Partial Reconstruction
- $\bar{B} \to D\ell\bar{\nu}$ Branching Fractions and Form Factor Parameters

Charm Physics:

- Measurement of the Decay Asymmetry Parameter in $\Xi_c^0 \to \Xi^-\pi^+$ and $\Xi^- \to \Lambda\pi^-$ and a Search for Direct CP Violation in Hyperon Decays
- Improved Measurement of the Pseudo-Scalar Decay Constant f_{Ds}

Tau Physics:

- Resonance Structure of $\tau^- \to K^-\pi^+\pi^-\nu_\tau$ Decays
- First Search for CP Violation in Tau Lepton Decay
- A Limit on the Mass of the ν_τ

Upsilon Physics:

- Υ Dipion Transitions at Energies near the $\Upsilon(4S)$
- Measurement of the Mass Splittings between the $B\bar{B}$ $\chi_{b,J}$ States.

This is just a sampling of CLEO's diverse activities. There are also many other new (i.e., not merely update) analyses underway.

12 Conclusion

Much of CLEO B Physics revolves around te CK CKM elements $|V_{cb}|$, $|V_{ub}|$ will be measured › even way, CLEO is also pioneering important techiques l efforts to explore the CP-violating aspects o the C a comprehensive set of rare B decay searchs; mai including some surprises, such as $B \to \eta' l$. It i decays is needed to get at the interesting physics di diagrams that contribute to these processes. CLEO'; by the time our run ends for CLEOIII instalition; for most B physics topics.

CLEO is also a major force in charm phyics (b physics, Upsilon physics, and two-photon physics. make use of a silicon vertex detector at the Υ4S), a three future B factories. Our own entry in th B fa online in 1999.

Current preprints and other information ai avail URL: http://www.lns.cornell.edu/public/CLEO/ . B no doubt be more exciting new results from CLEO tion concerning the impressive accomplishmats of available at http://www.lns.cornell.edu/publicCESR

13 Acknowledgments

Many thanks to my CLEO colleagues for the hard and especially to those who supplied figures ad oth these proceedings. I apologize for limiting m refere tal work; additional references should be easy obta

References

[1] CLEO Collaboration, Y. Kubota *et al.*, Nucl. Instrum. Methods Phys. Res., Sec. A **320**, 66 (1992).

[2] CLEO Collaboration, T. S. Hill, Nucl. Instrum. Methods Phys. Res., Sec. A **418**, 32 (1998).

[3] CLEO Collaboration, R. A. Briere, "Tracking in Helium-Based Gases: Present and Future B Factories," to appear in the *Proceedings of the Seventh International Symposium on Heavy Flavor Physics*, Santa Barbara, CA, July 1997.

[4] CLEO Collaboration, J. Bartelt *et al.*, Phys. Rev. Lett. **71**, 4111 (1993).

[5] CLEO Collaboration, J. P. Alexander *et al.*, Phys. Rev. Lett. **77**, 5000 (1996).

[6] CLEO Collaboration, C. P. Jessop *et al.*, CLEO CONF 98-18; ICHEP 855.

[7] CLEO Collaboration, B. Barish *et al.*, Phys. Rev. Lett. **76**, 1570 (1996).

[8] CLEO Collaboration, B. Barish *et al.*, Phys. Rev. D **51**, 1014 (1995).

[9] CLEO Collaboration, J. Bartelt *et al.*, CLEO CONF 98-21; ICHEP 1013.

[10] CLEO Collaboration, C. P. Jessop *et al.*, Phys. Rev. Lett. **79**, 4533 (1997).

[11] CLEO Collaboration, M. Artuso *et al.*, Phys Rev. Lett. **82**, 3020 (1999).

[12] CLEO Collaboration, M. Athanas *et al.*, Phys. Rev. Lett. **80**, 5493 (1998).

[13] CLEO Collaboration, G. Bonvicini *et al.*, CLEO CONF 98-23; ICHEP 852.

[14] CLEO Collaboration, R. Godang *et al.*, Phys. Rev. Lett. **80**, 3456 (1998).

[15] CLEO Collaboration, B. H. Behrens *et al.*, Phys. Rev. Lett. **80**, 3710 (1998).

[16] CLEO Collaboration, T. Bergfeld *et al.*, Phys. Rev. Lett. **81**, 272 (1998).

[17] CLEO Collaboration, D. M. Asner *et al.*, Phys. Rev. **D53**, 1039 (1996).

[18] CLEO Collaboration, B. H. Behrens *et al.*, CLEO CONF 98-09; ICHEP 860.

[19] CLEO Collaboration, M. Artuso *et al.*, CLEO CONF 98-20; ICHEP 858.

[20] CLEO Collaboration, S. Chan *et al.*, CLEO CONF 98-24; ICHEP 1073.

[21] CLEO Collaboration, M. S. Alam *et al.*, Phys. Rev. Lett. **74**, 2885 (1995).

[22] CLEO Collaboration, S. Glenn *et al.*, CLEO CONF 98-17; ICHEP 1011.

[23] K. Chetyrkin, M. Misiak, and M. Munz, Phys. Lett. **B400**, 206 (1997), E: ibid., **B425**, 414 (1998).

[24] CLEO Collaboration, R. Ammar *et al.*, Phys. Rev. Lett., **71**, 674 (1993).

[25] CLEO Collaboration, K. W. Edwards *et al.*, CLEO CONF 95-6; EPS0160.

[26] CLEO Collaboration, S. Glenn *et al.*, Phys. Rev. Lett. **80**, 2289 (1998).

[27] CLEO Collaboration, R. Godang *et al.*, CLEO CONF 98-22; ICHEP 1012.

[28] CLEO Collaboration, Phys. Rev. Lett. **82**, 4586 (1999). An earlier version of this work is detailed in: CLEO Collaboration, S. J. Richichi *et al.*, CLEO CONF 98-15; ICHEP 864.

[29] CLEO Collaboration, D. Cinabro *et al.*, Phys. Rev. Lett. **72**, 1406 (1994).

[30] CLEO Collaboration, C. P. Jessop *et al.*, Phys. Rev. Lett. **82**, 492 (1999).

[31] CLEO Collaboration, M. Athanas *et al.*, CLEO CONF 98-10; ICHEP 866.

[32] CLEO Collaboration, T. E. Coan *et al.*, CLEO CONF 98-19, ICHEP98 976.

[33] CLEO Collaboration, R. Godang *et al.*, Phys. Rev. Lett. **79**, 3829 (1997).

[34] CLEO Collaboration, M. S. Alam *et al.*, Phys. Rev. Lett. **81**, 3328 (1998).

[35] Review of Particle Physics, C. Caso *et al.*, Eur. Phys. J. C **3** 1 (1998).